Biophysical Journal Volume 109 July 2015 76–84

Article

Synaptobrevin Transmembrane Domain Influences Exocytosis by Perturbing Vesicle Membrane Curvature

Che-Wei Chang[1] and Meyer B. Jackson[1,*]
[1]Department of Neuroscience, Physiology Graduate Training Program, University of Wisconsin, Madison, Wisconsin

ABSTRACT Membrane fusion requires that nearly flat lipid bilayers deform into shapes with very high curvature. This makes membrane bending a critical force in determining fusion mechanisms. A lipid bilayer will bend spontaneously when material is distributed asymmetrically between its two monolayers, and its spontaneous curvature (C_0) will influence the stability of curved fusion intermediates. Prior work on Ca^{2+}-triggered exocytosis revealed that fusion pore lifetime (τ) varies with vesicle content (Q), and showed that this relation reflects membrane bending energetics. Lipids that alter C_0 change the dependence of τ on Q. These results suggested that the greater stability of an initial exocytotic fusion pore associated with larger vesicles reflects the need to bend more membrane during fusion pore dilation. In this study, we explored the possibility of manipulating C_0 by mutating the transmembrane domain (TMD) of the vesicle membrane protein synaptobrevin 2 (syb2). Amperometric measurements of exocytosis in mouse chromaffin cells revealed that syb2 TMD mutations altered the relation between τ and Q. The effects of these mutations showed a striking periodicity, changing sign as the structural perturbation moved through the inner and outer leaflets. Some glycine and charge mutations also influenced the dependence of τ on Q in a manner consistent with expected changes in C_0. These results suggest that side chains in the syb2 TMD influence the kinetics of exocytosis by perturbing the packing of the surrounding lipids. The present results support the view that membrane bending occurs during fusion pore expansion rather than during fusion pore formation. This supports the view of an initial fusion pore through two relatively flat membranes formed by protein.

INTRODUCTION

During membrane fusion, lipid bilayers must transiently assume shapes with very high curvature. This curvature comes at a significant energy cost, and thus the energetics of membrane bending plays a major role in defining the energy landscape of fusion and dictating the nature of the structural transitions that can take place. In catalyzing membrane fusion, proteins must contort lipid bilayers and deform them into shapes along the fusion pathway (1,2). Proteins can thus accelerate fusion by remodeling lipid bilayers into shapes approaching those of high-energy fusion intermediates. Studies of the membrane bending activity of proteins can provide valuable information for hypotheses about lipid structures along the fusion pathway. Likewise, studies of the influence of membrane bending energy on distinct kinetic steps of fusion can guide how investigators incorporate membrane bending into a detailed kinetic mechanism.

Membrane fusion creates a lipidic fusion pore formed by highly curved membranes shaped roughly like an hourglass. A substantial amount of energy is required to bend membranes into such a structure, and theoretical analysis indicates that this energy varies dramatically with the spontaneous curvature, C_0, of a lipid bilayer (3–6). Thus, the sensitivity of fusion to manipulations of C_0 provides insight into the composition of the fusion pore. Experiments examining the effect of cone-shaped lipids on viral fusion demonstrated the early formation of a lipidic fusion pore (7); however, Zhang and Jackson (8) found that such lipids had the opposite effect on Ca^{2+}-triggered exocytosis. They showed that the initial fusion pores of exocytosis had longer lifetimes when formed by larger vesicles, and this difference suggested that expanding a fusion pore formed by a large vesicle requires the bending of a larger area of membrane. Altering C_0 by adding cone-shaped lipids to the inner or outer leaflets of the cell membrane altered C_0 in opposite ways, and likewise changed the dependence of fusion pore lifetime on vesicle size in opposite ways. This work supported the hypothesis that an initial fusion pore composed of protein forms without significant membrane bending. Membranes become highly curved only when the fusion pore starts to dilate after a transition from protein to lipid. The hypothesis regarding an initial proteinaceous fusion pore received independent support from measurements of the sensitivity of fusion pore flux to mutations in SNARE protein transmembrane domains (TMDs) (9–11).

SNARE proteins catalyze biological fusion, and together with the Ca^{2+} sensor synaptotagmin these proteins constitute the essential molecular apparatus for Ca^{2+}-triggered exocytosis (12–14). The soluble cytoplasmic domains of synaptotagmin 1 bind to lipids in a Ca^{2+}-dependent manner (15) and penetrate lipid bilayers (16) to induce membrane

Submitted February 3, 2015, and accepted for publication May 11, 2015.
*Correspondence: mbjackso@wisc.edu
Editor: Brian Salzberg.

0006-3495/15/07/0076/9 $2.00
http://dx.doi.org/10.1016/j.bpj.2015.05.021

curvature (17,18). Integral membrane proteins can also deform membranes by applying force to their TMD. The isolated TMDs of SNARE proteins induce membrane fusion, but the mechanism of this activity remains unclear (19). Cone-shaped lipids incorporated asymmetrically into one leaflet of a bilayer alter C_0 and promote membrane bending (1,2). This raises the possibility that a TMD with nonuniformly distributed side-chain mass can act in a similar fashion. In this study, we explored this idea using mutations in the TMD of the vesicle SNARE protein synaptobrevin 2 (syb2). These mutations served as steric perturbations of bilayer structure at controlled depths to change the C_0 of each monolayer in both positive and negative directions. Using amperometry recording in chromaffin cells to probe the relation between vesicle size and fusion pore stability, we expressed various syb2 TMD mutations with side chains that perturbed the surrounding lipids. The impact of these mutations on C_0 varied depending on the depth of the side chain within the bilayer. The results indicated that the syb2 TMD influences the vesicle-size dependence of fusion pore stability in a manner that closely follows predictions based on the positions of perturbations of the inner and outer leaflets of the vesicle membrane. These data can be interpreted with the aid of a model in which an initial proteinaceous fusion pore expands to form a lipidic fusion pore.

MATERIALS AND METHODS

The materials and methods used in this work were described in a recent report from our laboratory (11).

Syb2 and cellubrevin double-knockout chromaffin cells

Syb2/cellubrevin double-knockout (DKO) mice were obtained by crossing syb2 heterozygous knockout (KO) and cellubrevin homozygous KO mice (20). The litters were one-quarter DKO (expressing neither syb2 nor cellubrevin), while the remaining three-quarters, taken as littermate controls, had one or two wild-type (WT) syb2 alleles and no cellubrevin. Chromaffin cells were cultured from embryonic day 17.5 (E17.5)–E18.5 embryos (8), and individual embryos were genotyped and cultured in separate dishes.

Molecular biology and virus transfection

Full-length mouse WT syb2 was amplified by PCR with the addition of *Xho*I 5′ and *Eco*RI 3′ restriction sites, and ligated into lentiviral vector pLox-CMV-EGFP (modified from pLox-Syn-Syn described previously (21)) to create a fusion construct with EGFP at the N-terminus of syb2 linked by the amino acid sequence SGLRSRG. Mutations were generated by QuikChange Site-Directed Mutagenesis (Agilent Technologies). WT and mutant constructs were confirmed by sequencing. HEK293T cells were cotransfected by the calcium phosphate method with three plasmids: pLox-CMV-EGFP-Syb2 or mutants, pCAG-VSVg (expressing the VSV-G envelope protein), and pCMVΔR8.91 (expressing the gag/pol proteins). The supernatant was collected 48–60 h later, filtered with 0.45-μm filter units, and centrifuged at 70,000 *g* for 2 h. The concentrated viral particles were resuspended with 100 μL phosphate-buffered saline and stored at −80°C. Chromaffin cells on each coverslip were infected with 10 μL of viral particles on the day of dissection.

Amperometry

Chromaffin cells (1–3 days in vitro) were bathed at room temperature (~22°C) in a solution consisting of (mM) 150 NaCl, 4.2 KCl, 1 NaH_2PO_4, 0.7 $MgCl_2$, 2 $CaCl_2$, 10 HEPES (pH 7.4). Amperometry recording with a VA-10 amplifier (ALA Scientific Instruments, Westbury, NY) was performed to detect catecholamine release, using 5-μm carbon fibers polarized to 650 mV. GFP fluorescence was visualized and used to detect infected cells. To elicit exocytosis, a depolarizing solution (identical to the bathing solution but with 105 mM KCl and 5 mM NaCl) was pressure ejected from an ~2-μm tipped micropipette positioned with a micromanipulator 10–15 μm from the cell. Amperometric current was recorded for 3 s, at which point the depolarizing solution was puffed for 6 s and recording was continued for another 14 s. This was repeated up to six times for each cell.

Recordings were analyzed with an in-house-written computer program that locates spikes and determines the prespike foot (PSF) duration according to a protocol described by Chow et al. (22). Only PSFs with durations of $\geq$0.75 ms associated with spikes of $\geq$20 pA were used for analysis. For each event that satisfied these criteria, we determined the PSF duration (τ) and the total area (Q) of the PSF + spike. Data were binned according the magnitude of Q, and Q and τ values within bins were averaged.

Statistics

Bar graphs generally display the mean ± error. For Q, the arithmetic means and standard errors of means are presented. For τ, the mean and error were determined from exponential fits to PSF lifetime distributions. Plots of $ln(1/\tau)$ versus $1/Q^{1/3}$ were fitted to lines, and the slopes are presented with the errors determined from linear regression. To compare slopes and PSF durations, one-way ANOVA and Dunnett's post test were used to identify the measurements from mutants that differed significantly from WT syb2.

RESULTS

Fusion pore stability, vesicle size, and membrane curvature

Amperometry detects catecholamine as it is released from chromaffin cells, and the exocytosis of individual vesicles produces brief spikes of amperometric current (23). Spikes are often preceded by PSFs that report the flux of catecholamine through nascent fusion pores (24–26). Fig. 1 *A* displays three single-vesicle release events recorded from mouse chromaffin cells. These examples illustrate the important relation between the duration (τ) of a PSF and the total area (Q), or charge, of an amperometry event: events with larger areas have longer-duration PSFs. Binning the Q values as described in Materials and Methods, and plotting the average τ of those events against Q revealed a strong positive correlation, with a ~10-fold variation in τ over the range of Q values observed (Fig. 1 *B*). Thus, the stability of a fusion pore is greater for vesicles containing more catecholamine.

Q scales with the volume of a vesicle calculated from its area as determined by capacitance measurement (27).

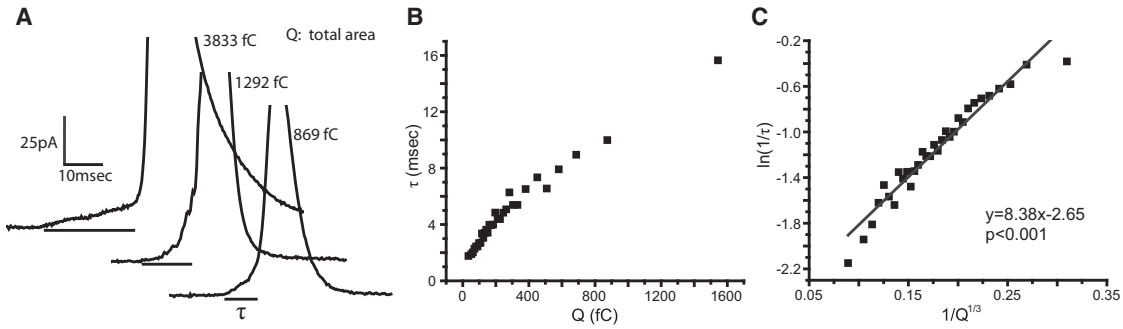

FIGURE 1 (*A*) Three selected amperometry traces from mouse chromaffin cells show larger events with longer PSFs. Q indicates the total integrated area of a spike and PSF; values are presented next to each trace. The PSF duration, τ, is indicated by a bar under each trace. (*B*) A plot of τ versus Q (3175 events, 100 events per bin). (*C*) The plot in (*B*) was transformed to $ln(1/\tau)$ versus $1/Q^{1/3}$. The linear fit and p value for linear regression are indicated.

Furthermore, $Q^{1/3}$ has a distribution that nearly overlies the distribution of the vesicle radius (8). Thus, $Q^{1/3}$ provides a quantity that scales as the vesicle radius. The elastic response to a bending force is measured in terms of curvature, and rates are generally exponential functions of energy. These considerations motivate the transformation of the τ-Q plot in Fig. 1 *B* to a $ln(1/\tau)$ − $1/Q^{1/3}$ plot. Data thus transformed were well fitted by linear regression (Fig. 1 *C*), suggesting that membrane elasticity contributes to an energy barrier of a fusion pore transition. Similar linear behavior was observed previously in such plots from PC12 cells and rat chromaffin cells (8).

Zhang and Jackson (8) previously explored the potential role of membrane bending in the relation between τ and Q by developing a continuum elasticity model based on the hypothesis that elastic resistance to fusion pore dilation is proportional to the amount of highly curved membrane within a lipidic fusion pore. Fig. 2 *A* illustrates this point by showing that the contact angle, θ, is larger with smaller vesicles, and the area of curved membrane within the fusion pore is correspondingly smaller. Mathematical analysis of this model yielded the following relation:

$$ln(1/\tau) = A + \frac{B}{R_v}\left(\frac{1}{R_r} - 3C_0 + R_r C_0^2\right), \qquad (1)$$

where R_v is the vesicle radius; A is the limiting energy (in units of kT) when R_v is very large; B is a parameter that depends on several quantities, such as the radius of the lipidic fusion pore and the membrane flexural rigidity; and R_r is related to the fusion pore geometry. The full version of this expression is Eq. 2 of Zhang and Jackson (8), and the derivation along with full expressions for A and B can be found in the appendix of that work. Equation 1 contains the salient aspects of this model. $ln(1/\tau)$ is proportional to $1/R_v$ (or $1/Q^{1/3}$), and the slope depends on C_0. Fitting of Eq. 1 to transformed τ-Q data, as presented in Fig. 1 *C*, provides a means of interpreting the relation between τ and Q in terms of C_0.

Tryptophan mutations in the syb2 TMD

The relation between τ and Q provides the basis for testing whether mutations in the TMD of a protein can alter C_0. Syb2 is the most abundant protein by copy number in synaptic vesicles (28) and is abundant in dense-core vesicles as well (11,29). Tryptophan has the largest side-chain volume of the natural amino acids, and when it faces the fusion pore lumen, it obstructs fusion pore flux (10,11). Therefore, we introduced tryptophan substitutions in the TMD (residues 95–116) with the expectation that when it faces the surrounding bilayer, it will create a bulge that will perturb the packing of lipids and modify C_0 of the vesicle membrane. Fig. 2 *B* illustrates how we can expect tryptophan mutations at different locations within a TMD to perturb the membrane in different ways. Mutations near the headgroups of the cytosolic leaflet or toward the end of the hydrocarbon chains of the luminal leaflet will both make C_0 negative. (Note that C_0 is taken as positive for the bending of membrane that occurs within the fusion pore in the plane perpendicular to the membranes. This is the shaded area in Fig. 2 *A*, and is commonly referred to as the meridian curvature. The parallel curvature in a fusion pore is opposite in sign and not visible in the projection shown in Fig. 2 *A*.) Conversely, mutations near the hydrocarbon chain ends of the cytosolic leaflet or near headgroups of the luminal leaflet will make C_0 positive (Fig. 2 *B*).

We generated tryptophan mutations through the syb2 TMD and expressed them in DKO chromaffin cells. WT and mutant syb2 constructs expressed at similar levels, targeted dense-core vesicles, and rescued secretion to similar degrees producing ~8-fold increases in Ca^{2+}-triggered exocytosis over untransfected DKO control cells (11). Thus, the fusion events observed can be attributed almost entirely to the expressed form of syb2 rather than endogenous vesicular SNARE protein. Fig. 2 *C* presents three representative $ln(1/\tau)$ − $1/Q^{1/3}$ plots that show that tryptophan substitution at position 96 increased the slope compared with the WT, whereas tryptophan substitution at position 101 decreased the slope. The slopes from WT

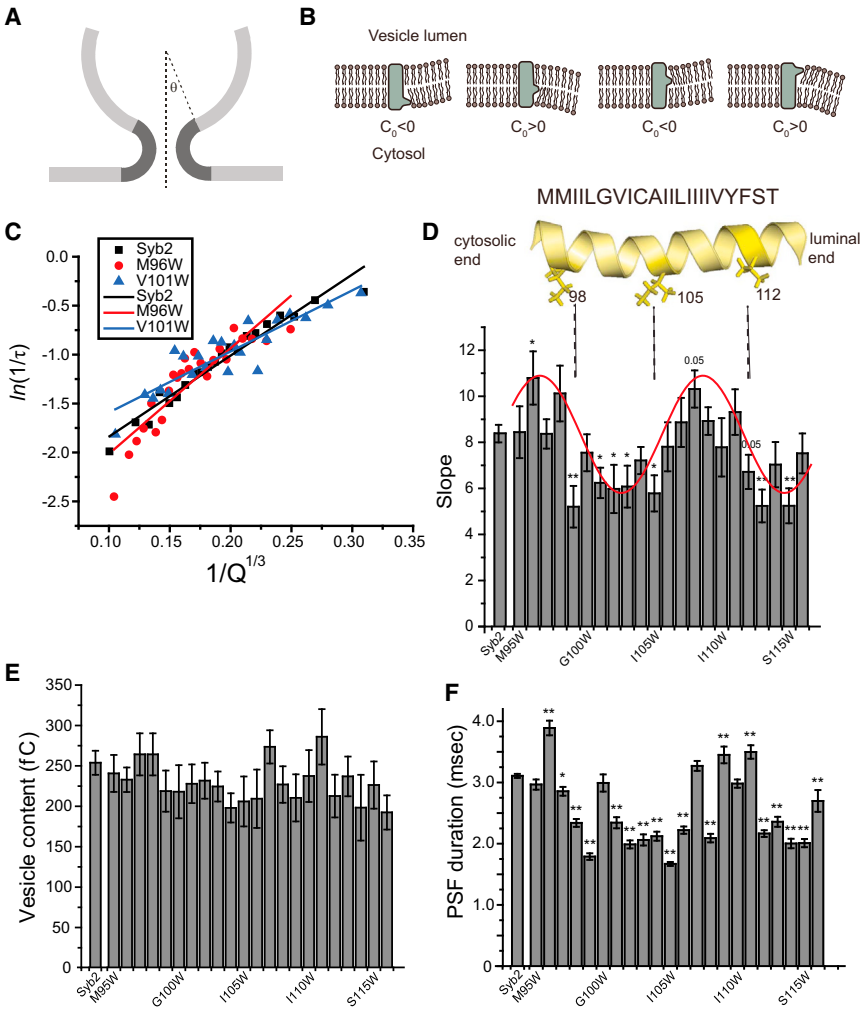

FIGURE 2 (*A*) Schematic depiction of how vesicle size influences the amount of curved membrane contained within a fusion pore. Smaller vesicles have larger contact angles (θ) and a lower area of highly curved membrane (*darker shading*). (*B*) Vesicle membrane curvature alterations by bulky tryptophan side chains at different positions in the syb2 TMD. The bilayer spontaneous curvature (C_0) is negative with the perturbation close to the headgroups of the cytoplasmic leaflet, and changes signs three times as the perturbation moves through the bilayer. (*C*) Representative plots of $ln(1/\tau)$ versus $1/Q^{1/3}$, with linear fits from cells expressing WT syb2, M96W, and V101W mutants. (*D*) Slopes from linear fits to $ln(1/\tau) - 1/Q^{1/3}$ plots from cells expressing WT syb2 and all tryptophan mutations in the syb2 TMD. The slopes increased with mutations at positions 96–98 and 107–111, and decreased with mutations at 99–105 and 112–116. Syb2 TMD (residues 95–116) is shown as a yellow ribbon model, and residues 98, 105, and 112 (shown as *sticks*) correspond roughly to positions where the effect on slope changes sign. A red sine wave drawn by eye through the data highlights the periodic changes in slope. Mutants that significantly altered the slope are indicated ($*p < 0.05$, $**p < 0.01$ compared with WT syb2; some p values of mutants are indicated). (*E* and *F*) Vesicle content (Q; *E*) and PSF duration (τ; *F*) for WT syb2 and all TMD tryptophan mutants ($*p < 0.05$, $**p < 0.01$ compared with WT syb2) are shown. To see this figure in color, go online.

syb2 and tryptophan mutants along the entire length of the TMD are displayed in Fig. 2 *D* as a function of residue number. These slopes varied by almost a factor of 2 and exhibited a striking periodic variation with position along the TMD (a sine wave in Fig. 2 *D* highlights this periodicity). Tryptophan substitutions at positions 96–98 and 107–111 increased the slopes, and tryptophan substitutions at 99–105 and 112–116 decreased the slopes. This trend corresponded well with the expected location of the mutations with respect to the headgroups and hydrocarbon chains of the two leaflets of the vesicle membrane (Fig. 2 *B*). Mutations increasing the slopes were predicted to make C_0 negative and mutations reducing the slopes were predicted to make C_0 positive.

None of the tryptophan mutations changed Q (Fig. 2 *E*), but the PSF lifetime changed with the position of the tryptophan substitution in a trend that roughly paralleled the changes in slope (Fig. 2 *F*). As previously seen with manipulations of C_0 using lipids (8), the fusion pore was usually stabilized (longer τ) as slopes increased and destabilized as slopes decreased. However, the trend was not perfect. For example, the mutant with tryptophan at residue 108 had a τ of 2.1 ms, whereas the mutants with tryptophan at the two neighboring positions had a τ of >3 ms (Fig. 2 *F*). By contrast, slopes from these mutations were very similar (Fig. 2 *D*). These disparities can be explained by noting that the slope effectively isolates membrane bending factors, whereas τ depends on additional factors such as specific contacts with other molecules (as discussed below; see Fig. 6).

Glycine mutations

As a contrast to tryptophan bulges, we introduced cavities by mutating to glycine. At positions 99, 101, and 102, where tryptophan reduced the slope, glycine left a slope similar to that of the WT (Fig. 3 *B*). At position 111, where tryptophan increased the slope, glycine produced a small, statistically insignificant decrease. At position 111, a plot for five different substitutions showed a statistically significant dependence on the side-chain volume (Fig. 3 *C*). However, in similar plots for substitutions at positions 99, 101, and 102, there was no statistically significant correlation

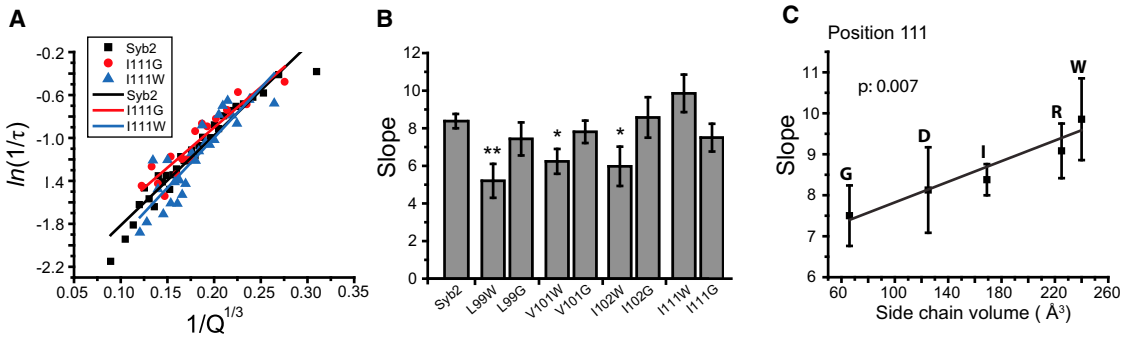

FIGURE 3 (*A*) Representative plots of $ln(1/\tau)$ versus $1/Q^{1/3}$ and linear fits from cells expressing WT syb2, I111G, and I111W mutations. (*B*) Slopes of $ln(1/\tau)$ versus $1/Q^{1/3}$ plots from cells expressing WT syb2, and glycine and tryptophan mutations at positions 99, 101, 102, and 111 ($*p < 0.05$, $**p < 0.01$ compared with WT syb2). Glycine mutations left slopes similar to that of the WT. (*C*) A plot of slope versus side-chain volume at position 111 exhibits a positive correlation. Linear regression yielded a p value of 0.007. The letters indicate the substitutions at position 111. To see this figure in color, go online.

(data not shown). Thus, vacancies produced by glycine had smaller effects than bulges produced by tryptophan.

Multiple mutations

To evaluate the additivity of the TMD mutations, we introduced four tryptophans (4W) or four glycines (4G) at positions 99, 101, 103, and 105. Single tryptophan mutations decreased the slopes at all of these sites, and we expected that quadruple mutations would enhance this effect. We also created a quadruple tryptophan mutation within the C-terminal half of the TMD (Cter-4W) at positions 108 and 110, where single tryptophan mutations increased the slope, and positions 112 and 113, where single tryptophan mutations decreased the slope (Fig. 2 *D*). The anticipated effects on C_0 of these quadruple mutants are illustrated in Fig. 4 *A*. Fig. 4 *B* presents the plots of $ln(1/\tau)$ versus $1/Q^{1/3}$ together with linear fits. The slope of the 4W mutant plot was indistinguishable from that of the single tryptophan mutants, indicating that the effects of these bulges were not additive (Fig. 4 *C*). The 4G mutant significantly increased the slope (Fig. 4 *C*), in contrast to the lack of effect of single glycine mutants (Fig. 3 *B*). The Cter-4W mutant did not alter the slope (Fig. 4 *C*), which may reflect the opposing effects of tryptophans at the different positions (Fig. 4 *A*). In summary, single mutations with the same effect showed additivity only with multiple cavity-inducing glycine substitutions, whereas tryptophan mutations with opposite effects canceled. These results indicate partial additivity in the effects of TMD mutations on the slopes of $ln(1/\tau)$ – $1/Q^{1/3}$ plots, which may in turn reflect partial additivity in the effects on C_0.

Electrostatic interactions

We tested charge mutations as a contrast to the mutations that create protrusions or vacancies. Single negatively and positively charged side chains at positions 99, 101, 102,

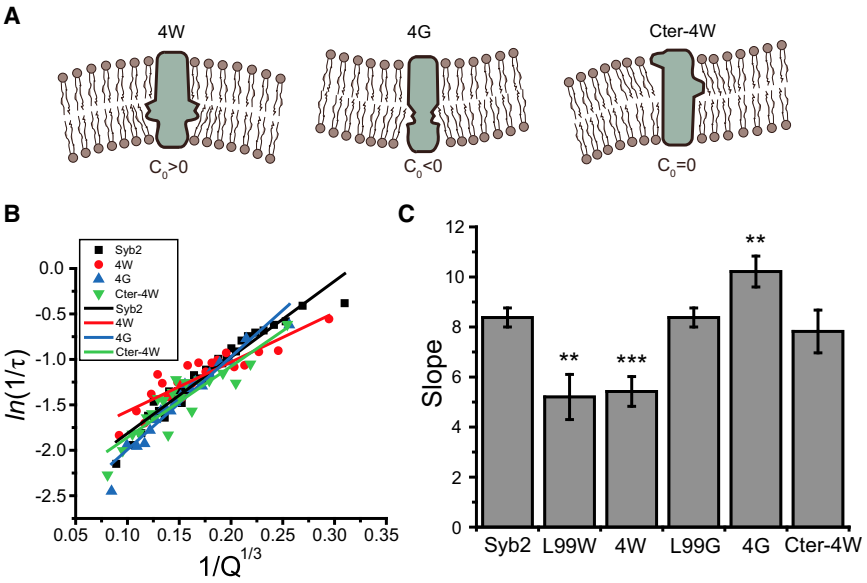

FIGURE 4 (*A*) Schematic depiction of the expected influence on vesicle membrane curvature of quadruple tryptophan (4W) and glycine (4G) mutations at positions 99, 101, 103, and 105, and a quadruple tryptophan mutation at positions 108, 110, 112, and 113 of the syb2 TMD (Cter-4W). The expected bilayer C_0 changes with different mutants. (*B*) Plots of $ln(1/\tau)$ versus $1/Q^{1/3}$ and linear fits from cells expressing WT syb2, 4G, 4W, and Cter-4W mutants. (*C*) Slopes of $ln(1/\tau)$ – $1/Q^{1/3}$ plots from cells expressing WT syb2, L99G, 4G, L99W, 4W, and Cter-4W ($**p < 0.01$, $***p < 0.001$ compared with WT syb2). To see this figure in color, go online.

and 111 failed to change the slopes of $ln(1/\tau) - 1/Q^{1/3}$ plots (Fig. 5, *A–D*). We also tested quadruple aspartate and arginine mutations (4D and 4R, respectively) at positions 99, 101, 103, and 105. The 4D mutant did not change the slope, but the 4R mutant significantly decreased the slope. This could reflect either the large side-chain volume of arginine or a water defect induced by burying charge within the hydrocarbon interior (see Discussion).

Slope correlations with PSF duration

Fig. 2 shows that tryptophan mutations influence the mean PSF duration as well as the slope of $ln(1/\tau)$ versus $1/Q^{1/3}$ plots. If the mutations alter fusion pore kinetics solely through an effect on membrane bending, our proposed mechanism (illustrated by the diagram in Fig. 2 *A*) would suggest that we should see parallel changes in these two quantities. Plots of PSF duration versus slope suggest that this is the case for substitutions with steric effects, such as tryptophan and glycine (Fig. 6 *A*), but not for charge mutations (Fig. 6 *B*). The correlation in Fig. 6 *A* is highly significant, with the points from the tryptophan and glycine mutations each falling on their own lines. The slope for the tryptophan mutations is approximately twice as steep as the slope for the glycine mutations. This correlation supports the idea that a common mechanism underlies the effects of tryptophan and glycine substitutions on fusion pore stability. However, two of the tryptophan mutations (residues 98 and 108) fell far from the best-fitting line. The most likely explanation for this observation is that these two residues are unique among the TMD residues in having an additional influence on fusion pore stability through a

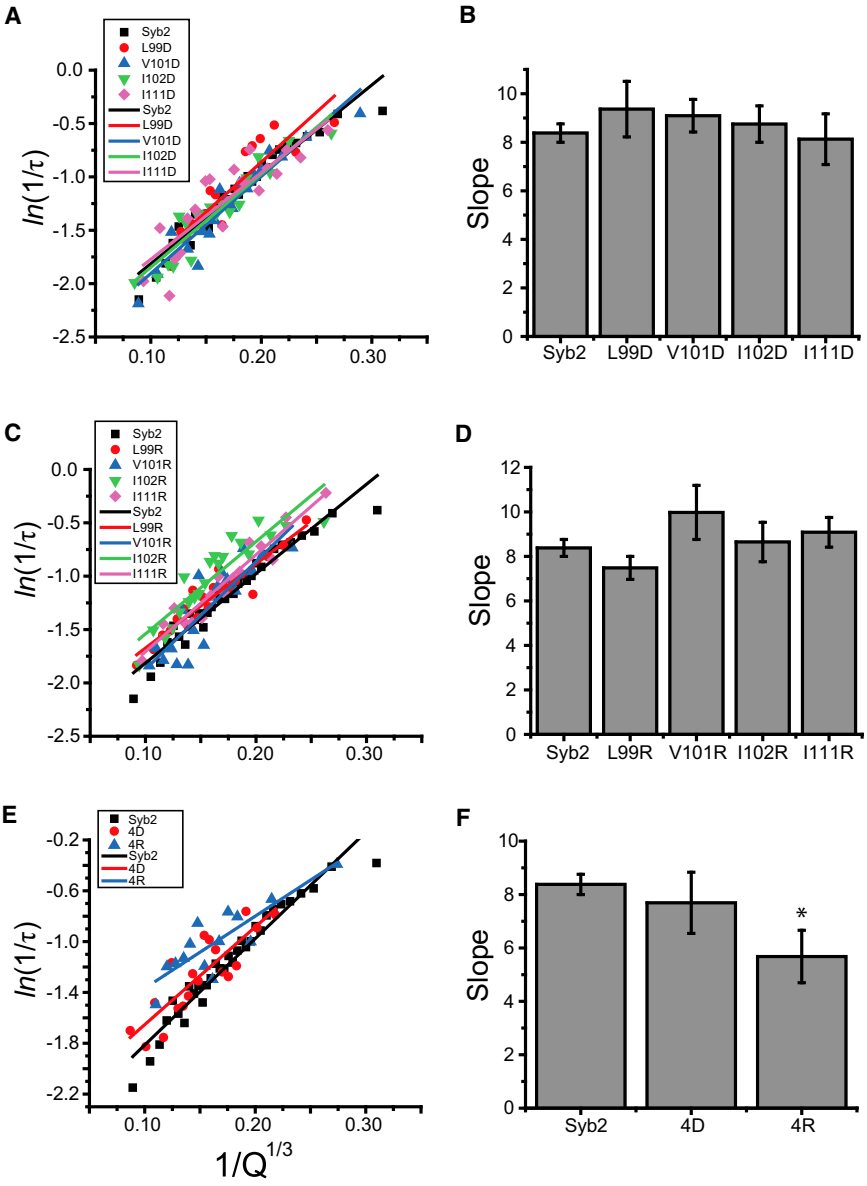

FIGURE 5 (*A* and *C*) Plots of $ln(1/\tau)$ versus $1/Q^{1/3}$ and linear fits from cells expressing aspartic acid or arginine at positions 99, 101, 102, and 111. (*B* and *D*) Slopes of the linear fits. (*E*) Plots of $ln(1/\tau)$ versus $1/Q^{1/3}$ and linear fits from cells expressing WT syb2, quadruple aspartic acid (4D), and quadruple arginine (4R) mutations at positions 99, 101, 103, and 105. (*F*) Slopes from (*E*); 4R significantly reduced the slope ($*p < 0.05$ compared with WT syb2). To see this figure in color, go online.

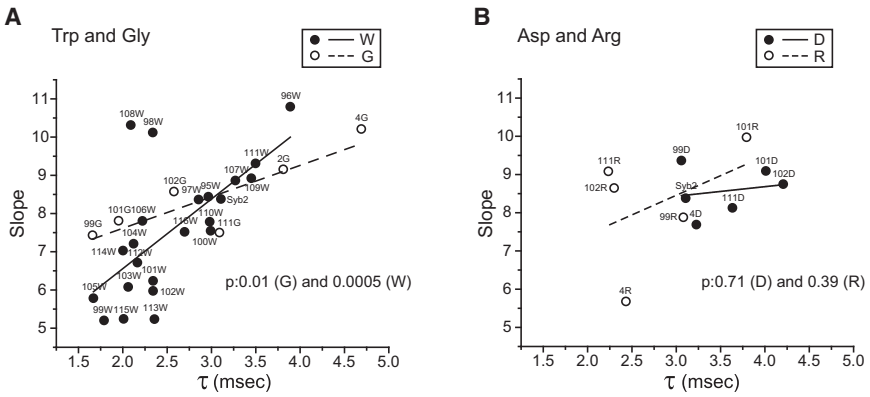

FIGURE 6 Slopes from plots of $ln(1/\tau)$ vs. $1/Q^{1/3}$ (as in Fig. 2 *C*) were plotted against mean PSF duration (τ). (*A*) Plot for tryptophan (W) and glycine (G) substitutions. (*B*) Plot for charged substitutions with arginine (R) and aspartate (D). The *p* values from linear regression indicate highly significant correlations for W and G, and no significant correlation for R and D. Two of the tryptophan mutations in (*A*) (residues 98 and 108) produce points far from the best-fitting line.

mechanism that is independent of membrane curvature. It is therefore intriguing that one of the residues, residue 98, is in close contact with the syntaxin TMD in a crystal structure of the cis-SNARE complex (31). The tryptophan substitution at this position could thus disrupt a zippering interaction with syntaxin. The interaction of the other residue that fell off the linear plot in Fig. 6 *A*, residue 108, remains unclear.

DISCUSSION

In this study, we explored the correlation between vesicle size and fusion pore stability, and used this relation to test TMD mutations as perturbants of membrane curvature. These perturbations enabled us to assess the role of membrane curvature in Ca^{2+}-triggered exocytosis. The longer τ with larger vesicles indicates that their fusion pores dilate more slowly, and the linear correlation between $ln(1/\tau)$ and $1/Q^{1/3}$ suggests that membrane bending contributes to the energy barrier for this kinetic process. We can interpret these results within the framework of a model in which the PSF represents flux through an initial proteinaceous fusion pore, and the PSF-to-spike transition reflects a conversion of a proteinaceous fusion pore to a lipidic fusion pore (8,32,33). For smaller vesicles, the contact angle between the vesicle and plasma membranes is larger, and a lipidic fusion pore contains less highly curved membrane (Fig. 2 *A*). This enables the proteinaceous fusion pore to convert to lipid more rapidly. The alternative scenario is that a PSF reflects flux through a lipidic fusion pore, and that the lipidic fusion pores of smaller vesicles expand more rapidly. Previous work distinguished between these two possibilities based on changes in C_0 due to cone-shaped lipids (8). Here we show that, like cone-shaped lipids, protein TMDs can alter C_0. The perturbations of C_0 by syb2 TMD mutations confirmed and extended the results obtained with lipids. Because our TMD mutations target different depths within a bilayer with much greater precision, we could test the full scope of influence of structural defects on C_0. It is important to point out that these experiments do not test the hypothesis that the syb2 TMD itself is a structural component of the fusion pore actually lining its wall. Here, the effects of the syb2 TMD were realized solely by its presence in the vesicle membrane. To change C_0, a TMD must be imbedded in the lipid bilayer. Any abundant vesicle-targeted TMD could exert such an influence, and the proteins that form the fusion pore are irrelevant to our assessment of TMD mutations. The critical point is that lipid bilayer C_0 can be altered by TMD mutations.

Tryptophan mutations at different locations in the syb2 TMD resulted in different effects on the slopes of $ln(1/\tau) - 1/Q^{1/3}$ plots. The variations in slope (Fig. 2 *D*) corresponded well with the location of the bulge and the expected effect on C_0 (Fig. 2 *B*). The slopes increased with tryptophan mutations near the headgroups of the cytosolic leaflet (positions 96–98) and the hydrocarbon chains of the luminal leaflet (positions 107–111) (Fig. 2, *C* and *D*). These mutations thus stabilized the fusion pore. This result is consistent with the prediction of a model based on an initial proteinaceous fusion pore (Fig. 7 *A*). Tryptophan mutations at positions 95–98 and 107–111 should decrease C_0 and bend the vesicle membrane away from the curvature seen in a lipidic fusion pore (Fig. 7 *B*, *left*), thus stabilizing the proteinaceous fusion pore (Fig. 7 *A*, *left*) and increasing the slope of $ln(1/\tau) - 1/Q^{1/3}$ plots. Conversely, tryptophan bulges at positions 99–105 and 112–116 should increase C_0 to bend the membrane toward the curvature seen in a lipidic pore (Fig. 7 *B*, *left*), thus decreasing the slope. Our data confirmed all of these predictions.

Small side-chain glycine substitutions induced smaller changes in slopes (Fig. 3 *B*), but a quadruple glycine mutation significantly increased the slope, as expected for a vacancy at that location. By contrast, the corresponding quadruple tryptophan mutation failed to show an additive effect (Fig. 4 *C*). Although the results are generally consistent with the anticipated effects on C_0, the reasons for the weaker effects of single cavities, and the difference in additivity of effects of cavities versus protrusions are not clear. Charged side-chain substitutions failed to alter the slopes, with the exception of the quadruple 4R mutation, which decreased the slope. Because arginine has a large side chain, the effect could be steric. However, burying charges in a membrane can also distort the bilayer structure by producing water

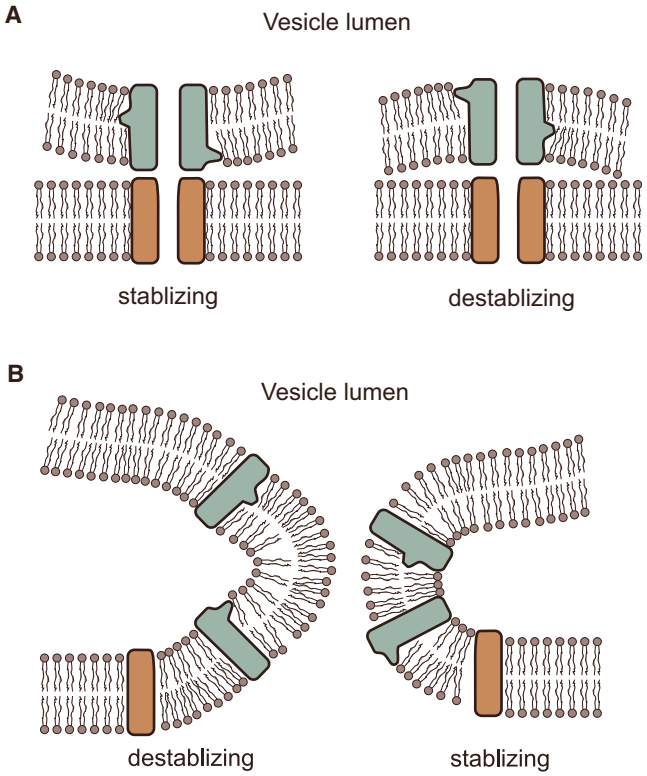

FIGURE 7 Schematic depiction of how fusion pore stability is influenced by bulky tryptophan side chains at different positions in a TMD. The perturbations illustrated in Fig. 2 *B* are incorporated into models for proteinaceous and lipidic fusion pores. (*A*) A proteinaceous initial fusion pore. Left: tryptophan creates a bulge around the headgroups of the cytosolic leaflet and the ends of hydrocarbon chains of the luminal leaflet of the vesicle membrane to maintain the vesicle curvature and stabilize the initial proteinaceous fusion pore. Right: tryptophans near the luminal leaflet headgroups and cytosolic leaflet hydrocarbon chain ends destabilize the proteinaceous pore. (*B*) A lipidic fusion pore. Left: tryptophan bulges as shown in (*A*) (*left*) introduce curvature opposite to that of the surrounding lipids to destabilize the lipidic pore. Right: tryptophan bulges as shown in (*A*) (*right*) pack well into the curvature of the surrounding lipid bilayers and stabilize the lipidic pore. To see this figure in color, go online.

defects that reduce the distance of a buried charge to bulk water (34,35). In general, positive charges are more difficult to move into the interior of a lipid bilayer. The introduction of these charges in the N-terminal half of the syb2 TMD can be interpreted in terms of a bilayer defect in the cytosolic face of the vesicle membrane that increases C_0.

Manipulating C_0 with protein TMD mutations yielded results consistent with the results of lipid manipulations (8). The defects induced by tryptophan bulges and glycine cavities corresponded well with the various extracellular and intracellular additions of oleic acid and lysophosphatidylcholine, and intracellular phosphatidylserine. Both protein and lipid perturbations for which we expected favorable packing into the curved membrane of a lipidic fusion pore destabilized the PSF, and perturbations for which we expected unfavorable packing stabilized the PSF. Extracellular lysophosphatidylcholine destabilized exocytotic fusion pores (8) but stabilized viral fusion pores (7), indicating fundamentally different mechanisms of membrane fusion in the two processes.

Previous work showed that mutations in the syntaxin TMD altered flux through initial fusion pores, implicating the syntaxin TMD as a structural component of the fusion pore through the plasma membrane (9,10). More recent experiments with syb2 implicated its TMD as a structural component of the fusion pore through the vesicle membrane (11). However, kiss-and-run events can give rise to amperometry spikes (36) and allow the loss of vesicle membrane (37,38). These results suggest that larger lipidic fusion pores can reseal, as indicated by capacitance flickers in protein-free systems (39). Lipid mixing can precede content mixing, and hemifusion intermediates form during SNARE-mediated liposome fusion assays. A TMD-truncated yeast v-SNARE protein or low copy numbers of yeast v-SNAREs impaired inner leaflet lipid mixing (40). Syntaxin and syb2 were shown to mediate hemifusion in liposome and cell fusion assays, and GPI-linked SNAREs produced only hemifusion (41). The TMDs of a single SNARE complex cannot form a channel, but can promote very low levels of liposome fusion (42). Although hemifusion intermediates form in a variety of situations, the fusion rates are generally slow. The proteinaceous fusion pore may be an adaptation for speed and specificity during synaptic transmission. The issue remains controversial, and composite fusion pores with both protein and lipid have been proposed (43,44). A proteinaceous fusion pore remains the most parsimonious interpretation of the effects of TMD mutations on both fusion pore flux and fusion pore stability. Resolution of this issue will probably require direct structural studies of exocytotic intermediates.

AUTHOR CONTRIBUTIONS

C.-W.C. carried out the experiments and analyzed the data. C.-W.C. and M.B.J. designed the research and wrote the manuscript.

ACKNOWLEDGMENTS

This work was funded by NIH grant NS044057.

REFERENCES

1. Chernomordik, L. V., and M. M. Kozlov. 2008. Mechanics of membrane fusion. *Nat. Struct. Mol. Biol.* 15:675–683.

2. Zimmerberg, J., and M. M. Kozlov. 2006. How proteins produce cellular membrane curvature. *Nat. Rev. Mol. Cell Biol.* 7:9–19.

3. Markin, V. S., and J. P. Albanesi. 2002. Membrane fusion: stalk model revisited. *Biophys. J.* 82:693–712.

4. Kozlovsky, Y., and M. M. Kozlov. 2002. Stalk model of membrane fusion: solution of energy crisis. *Biophys. J.* 82:882–895.

5. Katsov, K., M. Müller, and M. Schick. 2004. Field theoretic study of bilayer membrane fusion. I. Hemifusion mechanism. *Biophys. J.* 87:3277–3290.
6. Jackson, M. B. 2009. Minimum membrane bending energies of fusion pores. *J. Membr. Biol.* 231:101–115.
7. Razinkov, V. I., G. B. Melikyan, …, F. S. Cohen. 1998. Effects of spontaneous bilayer curvature on influenza virus-mediated fusion pores. *J. Gen. Physiol.* 112:409–422.
8. Zhang, Z., and M. B. Jackson. 2010. Membrane bending energy and fusion pore kinetics in Ca(2+)-triggered exocytosis. *Biophys. J.* 98:2524–2534.
9. Han, X., and M. B. Jackson. 2005. Electrostatic interactions between the syntaxin membrane anchor and neurotransmitter passing through the fusion pore. *Biophys. J.* 88:L20–L22.
10. Han, X., C. T. Wang, …, M. B. Jackson. 2004. Transmembrane segments of syntaxin line the fusion pore of Ca^{2+}-triggered exocytosis. *Science.* 304:289–292.
11. Chang, C. W., E. Hui, …, M. B. Jackson. 2015. A structural role for the synaptobrevin 2 transmembrane domain in dense-core vesicle fusion pores. *J. Neurosci.* 35:5772–5780.
12. Chapman, E. R. 2008. How does synaptotagmin trigger neurotransmitter release? *Annu. Rev. Biochem.* 77:615–641.
13. Südhof, T. C., and J. E. Rothman. 2009. Membrane fusion: grappling with SNARE and SM proteins. *Science.* 323:474–477.
14. Jahn, R., and D. Fasshauer. 2012. Molecular machines governing exocytosis of synaptic vesicles. *Nature.* 490:201–207.
15. Brose, N., A. G. Petrenko, …, R. Jahn. 1992. Synaptotagmin: a calcium sensor on the synaptic vesicle surface. *Science.* 256:1021–1025.
16. Chapman, E. R., and A. F. Davis. 1998. Direct interaction of a Ca^{2+}-binding loop of synaptotagmin with lipid bilayers. *J. Biol. Chem.* 273:13995–14001.
17. Hui, E., C. P. Johnson, …, E. R. Chapman. 2009. Synaptotagmin-mediated bending of the target membrane is a critical step in Ca(2+)-regulated fusion. *Cell.* 138:709–721.
18. Martens, S., M. M. Kozlov, and H. T. McMahon. 2007. How synaptotagmin promotes membrane fusion. *Science.* 316:1205–1208.
19. Langosch, D., J. M. Crane, …, J. Reed. 2001. Peptide mimics of SNARE transmembrane segments drive membrane fusion depending on their conformational plasticity. *J. Mol. Biol.* 311:709–721.
20. Borisovska, M., Y. Zhao, …, D. Bruns. 2005. v-SNAREs control exocytosis of vesicles from priming to fusion. *EMBO J.* 24:2114–2126.
21. Gascón, S., J. A. Paez-Gomez, …, F. G. Scholl. 2008. Dual-promoter lentiviral vectors for constitutive and regulated gene expression in neurons. *J. Neurosci. Methods.* 168:104–112.
22. Chow, R. H., and L. von Rüden. 1995. Electrochemical detection of secretion from single cells. *In* Single-Channel Recording. B. Sakmann and E. Neher, editors. Plenum Press, New York, pp. 245–275.
23. Wightman, R. M., J. A. Jankowski, …, O. H. Viveros. 1991. Temporally resolved catecholamine spikes correspond to single vesicle release from individual chromaffin cells. *Proc. Natl. Acad. Sci. USA.* 88:10754–10758.
24. Chow, R. H., L. von Rüden, and E. Neher. 1992. Delay in vesicle fusion revealed by electrochemical monitoring of single secretory events in adrenal chromaffin cells. *Nature.* 356:60–63.
25. Jankowski, J. A., T. J. Schroeder, …, R. M. Wightman. 1993. Temporal characteristics of quantal secretion of catecholamines from adrenal medullary cells. *J. Biol. Chem.* 268:14694–14700.
26. Wang, C.-T., R. Grishanin, …, M. B. Jackson. 2001. Synaptotagmin modulation of fusion pore kinetics in regulated exocytosis of dense-core vesicles. *Science.* 294:1111–1115.
27. Gong, L. W., I. Hafez, …, M. Lindau. 2003. Secretory vesicles membrane area is regulated in tandem with quantal size in chromaffin cells. *J. Neurosci.* 23:7917–7921.
28. Takamori, S., M. Holt, …, R. Jahn. 2006. Molecular anatomy of a trafficking organelle. *Cell.* 127:831–846.
29. Brunner, Y., Y. Couté, …, J. C. Sanchez. 2007. Proteomics analysis of insulin secretory granules. *Mol. Cell. Proteomics.* 6:1007–1017.
30. Reference deleted in proof.
31. Stein, A., G. Weber, …, R. Jahn. 2009. Helical extension of the neuronal SNARE complex into the membrane. *Nature.* 460:525–528.
32. Jackson, M. B. 2010. SNARE complex zipping as a driving force in the dilation of proteinaceous fusion pores. *J. Membr. Biol.* 235:89–100.
33. Jackson, M. B. 2011. Inferring structures of kinetic intermediates in Ca(2+)-triggered exocytosis. *Curr. Top. Membr.* 68:185–208.
34. MacCallum, J. L., W. F. Bennett, and D. P. Tieleman. 2007. Partitioning of amino acid side chains into lipid bilayers: results from computer simulations and comparison to experiment. *J. Gen. Physiol.* 129: 371–377.
35. Choe, S., K. A. Hecht, and M. Grabe. 2008. A continuum method for determining membrane protein insertion energies and the problem of charged residues. *J. Gen. Physiol.* 131:563–573.
36. Alés, E., L. Tabares, …, G. Alvarez de Toledo. 1999. High calcium concentrations shift the mode of exocytosis to the kiss-and-run mechanism. *Nat. Cell Biol.* 1:40–44.
37. Monck, J. R., G. Alvarez de Toledo, and J. M. Fernandez. 1990. Tension in secretory granule membranes causes extensive membrane transfer through the exocytotic fusion pore. *Proc. Natl. Acad. Sci. USA.* 87:7804–7808.
38. Taraska, J. W., and W. Almers. 2004. Bilayers merge even when exocytosis is transient. *Proc. Natl. Acad. Sci. USA.* 101:8780–8785.
39. Chanturiya, A., L. V. Chernomordik, and J. Zimmerberg. 1997. Flickering fusion pores comparable with initial exocytotic pores occur in protein-free phospholipid bilayers. *Proc. Natl. Acad. Sci. USA.* 94:14423–14428.
40. Xu, Y., F. Zhang, …, Y. K. Shin. 2005. Hemifusion in SNARE-mediated membrane fusion. *Nat. Struct. Mol. Biol.* 12:417–422.
41. Giraudo, C. G., C. Hu, …, J. E. Rothman. 2005. SNAREs can promote complete fusion and hemifusion as alternative outcomes. *J. Cell Biol.* 170:249–260.
42. van den Bogaart, G., M. G. Holt, …, R. Jahn. 2010. One SNARE complex is sufficient for membrane fusion. *Nat. Struct. Mol. Biol.* 17:358–364.
43. Jackson, M. B., and E. R. Chapman. 2006. Fusion pores and fusion machines in Ca^{2+}-triggered exocytosis. *Annu. Rev. Biophys. Biomol. Struct.* 35:135–160.
44. Fang, Q., K. Berberian, …, M. Lindau. 2008. The role of the C terminus of the SNARE protein SNAP-25 in fusion pore opening and a model for fusion pore mechanics. *Proc. Natl. Acad. Sci. USA.* 105:15388–15392.